Mon. Not. R. Astron. Soc. **000**, 1–9 (1999) Printed 22 October 2018 (MN LATEX style file v1.4)

Gamma Ray Bursts with peculiar temporal asymmetry

Gustavo E. Romero[1,⋆], Diego F. Torres[2], I. Andruchow[3], Luis A. Anchordoqui[2] & Bennett Link[4,†]
[1] *Instituto Argentino de Radioastronomía, C.C. 5, 1894, Villa, Elisa, Argentina*
2Departamento de Física, Universidad Nacional de La Plata, C.C. 67, (1900) La Plata, Argentina
[3] *Facultad de Ciencias Astronómicas y Geofísicas, Paseo del Bosque S/N, (1900) La Plata, Argentina*
[4] *Montana State University, Department of Physics, Bozeman, MT 59717, USA*

22 October 2018

ABSTRACT
Based on the study of temporal asymmetry of 631 gamma ray bursts from the BATSE 3B catalog by Link and Epstein [Ap J 466, 764 (1996)], we identify the population of bursts whose rising times are longer than their decays, thus showing atypical profiles. We analyse their sky distribution, morphology, time-space clustering and other average properties and compare them with those associated with the bulk of the bursts. We show how most of the peculiar bursts analysed are consistent with recent fireball models, but a fraction of bursts ($\sim 4\%$ of the total sample) appear to be inconsistent.

Key words: gamma rays: bursts

1 INTRODUCTION

During more than 25 years, the origin of gamma ray bursts (GRBs) has been, perhaps, the deepest and most persistent problem in astrophysics. However, with the advent of the Compton Gamma Ray Observatory (CGRO) and its Burst and Transient Source Experiment (BATSE) in 1991, a new phase in the research of GRBs started. In seven years of operation, BATSE has accumulated a database of more than 2000 observations. The angular distribution of these bursts is isotropic within the statistical limits, and the paucity of faint bursts implies that we are seeing to near the edge of the source population (e.g. Meegan et al. 1992, Fishman & Meegan 1995). Both effects, isotropy and non-homogeneity in the distribution, strongly suggest a cosmological origin of the phenomenon. In support of this conclusion, absorption lines (Fe II and Mg II) in the optical counterpart of GRB 970508 have been detected with a redshift of $z = 0.835$. Along with the absence of Lyman-α forest features in the spectra, these results imply that the burst source is located at $0.835 \leq z \leq 2.3$ (Metzger et al. 1997).

The energy required to generate cosmological bursts is as high as 10^{51} erg s^{-1}. The very short timescale observed in the time profiles indicate an extreme compactness that implies a source initially opaque (because of $\gamma\gamma$ pair creation) to γ-rays. The radiation pressure on the optically thick source drives relativistic expansion, converting internal energy into kinetic energy of the inflating shell. Baryonic pollution in this expanding flow can trap the radiation until most of the initial energy has gone into bulk motion with Lorentz factors of $\Gamma \geq 10^2 - 10^3$. The kinetic energy, however, can be partially converted into heat when the shell collides with the interstellar medium or when shocks within the expanding source collide with one another. The randomized energy can be then radiated by synchrotron radiation and inverse Compton scattering yielding non-thermal bursts with timescales of seconds. This fireball scenario has been developed by Cavallo and Rees (1978), Paczyński (1986), Goodman (1986), Mészáros and Rees (1993), Mészáros, Laguna and Rees (1993) and others. A comprehensive review is presented by Mészáros (1997).

The fireball model is a robust astrophysical scenario independent of the mechanism assumed for the original energy release. A popular mechanism is the merger of two collapsed stars in a binary system, for instance, two neutron stars or a neutron star and a black hole (see Narayan, Paczyński & Piran 1992, and references threin), although other processes have been suggested (e.g. Usov 1992, Carter 1992, Melia and Faterzzo 1992, Woosley 1993).

One important prediction of the fireball model, as well as by any explosive mechanism, is that individual burst profiles should be inherently asymmetric under time reversal, with a shorter rise time than the subsequent decay time. This is a natural consequence of a sudden particle energy increase (e.g. produced by a shock) and the slower radiative dissipation of the energy excess.

Time asymmetry in GRBs light curves has been discussed by several authors (e.g. Mitrofanov et al. 1994, Link et. al. 1993, Nemiroff et al. 1994). In particular, Nemiroff et

⋆ Member of CONICET. Email: romero@irma.iar.unlp.edu.ar
† Email: blink@dante.physics.montana.edu

al. (1994) showed that in the sample formed by those bursts with count rates greater than 1800 counts s^{-1} and durations longer than 1s detected by BATSE until 1993 March 10, there is a significant asymmetry in the bursts profiles in the sense that most bursts rise in a shorter time than they decay, in agreement with what is expected from a general fireball model. The most recent and complete study was made by Link and Epstein (1996). They took 631 GRBs from the BATSE 3B catalog, including both faint and bright bursts, and confirmed the global asymmetry in the burst profiles showing that about two thirds of the events display fluxes that rise faster than the subsequent fall. About 30% of the bursts, however, presented a peculiar asymmetry in the temporal profiles, with slower risings than decays.

In this paper we focus on this subsample of *peculiar asymmetric bursts* (PABs), which seems at first sight to conflict with some predictions of the simplest scenarios for fireballs. In particular, we shall discuss whether there are reasons to consider this subsample of GRBs as representative of a class of sources with different physical properties than other bursts. The structure of the paper is as follows. In Section 2 we define the sample and present the results of the symmetry analysis. We provide tables with the full results for PABs in order to allow identification of specific events. In Section 3 we study the sky distribution of the sample, while in Section 4 we investigate the level of positional coincidence (possible repetition) that PABs show. Finally, we discuss the implications of these results for theoretical models of GRBs.

2 SAMPLE AND SYMMETRY ANALYSIS

We have studied the sample of 631 bursts from the BATSE 3B catalog whose global symmetry properties were discussed by Link and Epstein (1996). This sample contains both faint and bright bursts, spanning a 200-fold range in peak flux. PREB plus DISC data types at 64 ms time resolution, with four energy channels, were used in the analysis.

The time asymmetry of the individual burst profiles was examined with the skewness function introduced by Link et al. (1993) and used in Link and Epstein's (1996) paper. This function is defined as

$$\mathcal{A} \equiv \frac{<(t-<t>)^3>}{<(t-<t>)^2>^{3/2}}. \qquad (1)$$

Here, angle brackets denote an average over the data sample, performed as

$$<g(t)> \equiv \frac{\sum_i (c_i - c_{th}) g(t_i)}{\sum_i (c_i - c_{th})}, \qquad (2)$$

where c_i is the measured number of counts in the ith bin, t_i is the time of the ith bin and c_{th} is a threshold level defined as,

$$c_{th} = f(c_p - b) + b. \qquad (3)$$

Here c_p stands for the peak (maximum) count rate, b is the background, and $f < 1$ is a fraction that will be fixed for the data set. Fixing f ensures that $\mathcal{A}$ is calculated to the same fraction of the peak flux relative to the background. Larger values of f emphasize the structure of the peak over the surrounding foothills. The normalization of $\mathcal{A}$ makes it independent of background, duration, and amplitude. It is equal to 0 in the case of symmetric bursts, greater than 0 for a burst whose peak rises more quickly than it falls and smaller than 0 in the opposite case. It is equal to 2 for an exact FRED (from *fast rise and exponential decay*) and to -2 for an exact anti-FRED. Four fixed values of f were analyzed: f_1=0.1, f_2=0.2, f_3=0.5 and f_4=0.67. The only requirement for a burst to be tested in each of the four f-values is that the number of bins whose c_i exceeds or equals c_{th} is at least three. Consequently, the size of the sample differs for each choice of f. The error bars in $\mathcal{A}$ represent 1σ deviations, calculated by randomizing the number of counts according to Poisson statistics and computing the variance of the asymmetry parameter for many trials.

In Tables 1 - 4 we show the results of the skewness analysis for those bursts that presented PAB behavior (i.e. $\mathcal{A} < 0$). Each table contains the peak flux, trigger number, burst type, value of the symmetry parameter for each f_i, and a classification of the bursts profiles according to the following scheme: S for single-peaked or spike-like bursts, M for multiply-peaked bursts, and C for complex or chaotic events. Regarding the burst types, events for which the $\mathcal{A}$ is negative for all f are labelled "1", whereas events for which the errors in $\mathcal{A}$ allow positive $\mathcal{A}$ for at least one value of f are denoted "2". In Fig. 1 we show specific examples of these profiles.

We found that 91 out of 631 bursts (14.4%) are PABs, *i.e.* do not present positive skewness for any f.‡ Only 28.5% of these bursts are single-peaked. The rest are multiply-peaked or complex events. Notice that most of S-type bursts are in Table 4. This is consistent with the analysis technique: a fast burst, typically lasting a couple of seconds, will have few points above the higher cut-offs and then, data for $\mathcal{A}_{f_2,f_3,f_4}$ will not be computed.

As we can see from Tables 1 - 4 as well as from Fig. 1, PABs exhibit a variety of temporal morphologies. If all of these events are produced by a single mechanism, then there should be a very wide range of boundary and initial conditions in the sources in order to generate such a plurality of profiles. With the aim of searching for differences between PABs and the more common bursts, we have computed average values of the hardness ratio and durations of type 1 PABs. These values are compared with similar estimates for those bursts with $\mathcal{A} > 0$ at all levels in Table 5. Due to the small number of bursts and the variety in their features, dispersions are so large that no conclusions can be drawn. However, in the light of current data, it is clear that no significant correlation is found between hardness ratio, or duration, with burst morphology.

3 SKY DISTRIBUTION

One of the most important results of BATSE is the discovery of that GRBs are isotropically distributed on the sky (see, however, Balazs et al. 1998). With the recent detection of high-redshifted absorption lines in the optical counterparts of individual bursts (Djorgovski et al. 1997, Metzger et al. 1997, van Paradjis et al. 1997) Galactic models appear to be

‡ 40 bursts out of these 91 are type 1.

finally ruled out. However, one could ask whether the distribution of PABs exhibits the same level of isotropy than that of the whole sample. It could be the case, for instance, that PABs have a different origin than other GRBs, and consequently, display a distinct distribution on the sky (e.g. there could be a statistically significant concentration of PABs in the supergalactic plane or within any superstructure).

In order to quantify the isotropy we followed the method developed by Briggs (1993). The dipole moment toward the Galactic center is $< \cos\theta >$, the mean of $\cos\theta_i$, where θ_i is the angle between the ith burst and the Galactic center. An excessively large value of $< \cos\theta >$ indicates a significant dipole moment towards the Galactic center. The quantity $< \sin^2 b - 1/3 >$ tests for a concentration in the Galactic plane or in the Galactic poles. The expected mean values of the two statistics are zero for an isotropic distribution and, if they are asymptotically gaussian distributed, i.e. if for a large number of bursts in the sample (N) they are gaussian distributed, the variances σ^2 are $1/3N$ and $4/45N$ respectively.

Briggs et al. (1996) noted that because the CGRO is in a low-Earth orbit, about one-third of the sky is blocked by the Earth causing a portion of the Galactic equator to be observed about 20% less than the poles. An additional effect is different exposure times between the Galactic south and north poles. These effects must be taken into account when computing the expected values of the statistics (Briggs et al. 1996). Location errors on particular bursts, however, have no impact on the isotropy characteristics because they are small compared with the large scale of anisotropies we are testing against.

Table 6 shows that the distribution of all PABs (Fig. 2) is consistent with perfect isotropy. The same is true for sub-samples of PABs. Some entries in Table 6 show small deviations from isotropy (quadrupole). However, the small number of events make the asymptotic gaussian distribution no longer valid, and one should compare with the study of Briggs et al. (1996) (see their Fig. 4a and b). Comparing with the values of σ that arise from the previous cited figures of the Briggs et al. work, we find, consequently, that there is no detectable anisotropy in the sky distribution of PABs and we see that the 1σ deviation from isotropy contains the values of all entries in Table 6.

4 TIME-SPACE CLUSTERING

Several time-space clustering analysis of different GRB-samples have come to contradictory conclusions about whether some GRBs repeat or not (e.g. Quashnock & Lamb 1993, Narayan & Piran 1993, Wang & Lingenfelter 1995, Petrosian & Efron 1995, Meegan et al. 1995). The most complete study on the subject until now, carried out by Tegmark et al. (1996), is based on the analysis of the angular power spectrum of 1120 bursts from BATSE 3B catalog. These authors found that the number of bursts that can be labelled as repeaters (considering just one repetition) is not larger than 5% at 99% confidence. The recent study of by Gorosabel et al. (1998), which combined data from different satellites, shows that at most 15.8% of the events detected by WATCH recur in the BATSE sample (at 94% confidence level). Despite the discussion in the literature, it seems clear that only a small fraction of the total number of GRBs could repeat over timescales of up to a few years.

However, if PABs have a different physical origin than other bursts, this subclass of bursts might exhibit time-space clustering. In fact, we find that 48 out of 91 PABs (52.7%) have companions within their location error boxes in the sample of 631 bursts. If we consider just bursts separated by less than 4^o, we find 40 possible repeaters (44% of the PAB-subsample); typically, the separation is about 2.5^o.

To estimate the statistical significance of these results, we have made a numerical study as follows. We have simulated 1500 sets of 91 random positions for PABs. In order to do this, we have made rotations on the celestial sphere sending a particular PAB with coordinates (l, b) to a new position (l', b'), which is obtained from the previous by seting $l' = l + R_1\, 360^o$ and $b' = b + R_2\, 90^o$, and using appropriate spherical boundary conditions. Here, R_1 and R_2 are different random numbers (between 0 and 1) which never repeat. Doing this for each event we get a new set of simulated PAB-positions. For this set we then compute the positional coincidence level with respect to the fixed $631 - 91$ GRBs coordinates. As in the real case, we shall assign a positional coincidence when two or more bursts are separated by less than 4^o. After making 1500 operations of this type (a larger number of simulations does not significantly modify the results) we can obtain the mean value of the expected number of positional coincidences and its σ. We obtain that for 91 GRBs, the average level of positional coincidences is 42.9 ± 4.7, which is entirely compatible with the observed result for PABs within 1σ.

We have repeated the process for the subset of 26 single-peaked PABs (those denoted by an S in Tables 1 - 4). These events represent about 4% of the whole sample and about 28.5% of the PAB subsample. 15 out of 26 bursts of this kind ($\sim$60%) present companions within error boxes of less than 4 degrees. We find that the average simulated positional coincidence level is 13.3 ± 2.5. That is, the real coincidence level is also compatible with the random result to within 1σ and no particular association appears obvious.

If we now take positional coincidences separated by less than 1^o, we find that 3 out of 26 single-peaked PABs have companions. Repeating the simulations in this case yields an expected chance association of 1 ± 1 events. This means that the real positional coincidence is only compatible with the random one to within 2σ. The number of events is of course too scarce to draw any conclusion, but if this is confirmed in a larger sample it would entail an excess of 3.8% repetitions above the result expected from chance associations (something compatible with already mentioned Tegmark et al.'s analyses).

As we shall see in the next section, spikes with peculiar asymmetry present problems for their interpretation within the standard fireballs models.

5 PABS AND THE FIREBALL MODELS

As mentioned in the introduction, GRBs profiles with $\mathcal{A} < 0$ are not expected from the simplest versions of the fireball model (i.e. a single expanding shell that acts as a gamma ray emitter during a brief time at some fixed radius from the central site of the explosion, e.g. Fenimore et al. 1996). However, one of the distinctive features of the fireball scenario is that the same basic mechanism can generate a variety of time profiles for different initial and boundary conditions. We now discuss whether these changes can provide the main types of PABs observed in the sample.

In Fig. 3 we show the profile of BATSE trigger #2450, which has negative skewness function for all values of f (see Table 1). This is a typical multiply-peaked burst, with a precursor at $t = 0$ and a series of peaks of increasing height that start about 35 s after the first signal. Individual peaks, when analysed with appropriate f, give $\mathcal{A} > 0$. Events of this kind can be understood as the effect of a mild baryon loaded fireball (Mészáros & Rees 1993). Even a small baryon contamination ($M_b \geq 10^{-9} M_\odot$) of the expanding pair-photon fireball is enough to trap the γ-rays until most of the initial energy is transformed into kinetic energy of the baryons. The fireball expands by radiation pressure and becomes optically thin to Thomson scattering when the optical depth drops below unity at a radius given by (Mészáros & Rees 1993),

$$r_p \sim 0.6 \times 10^{15} \theta^{-1} E_{51}^{1/2} \eta^{-1/2} \;\; \text{cm}, \quad (4)$$

where θ takes into account the possibility of channeling of the flow ($\theta \sim 1$ corresponds to spherical symmetry), E_{51} is the original energy release ($e^{\pm}, \gamma$) in units of 10^{51} erg, and $\eta = E_0/M_0 c^2$ is the initial radiation to the rest mass energy ratio in the fireball. At $r = r_p$, the γ-rays still trapped in the fireball can escape producing a burst (Cavallo & Rees 1978, Paczński 1986, Goodman 1986). As shown by Mészáros & Rees (1993), this burst should be rather weak, with an observed energy in gamma rays of, approximately,

$$E_p^{obs} \sim 7 \times 10^{47} \theta^{1/3} E_{51}^{1/2} \eta_3^{11/6} \;\; \text{erg}, \quad (5)$$

where $\eta_3 = 10^{-3}\eta$. This prompt, small burst will form a precursor that can last a few seconds. When the expanding relativistic shell collides with the interstellar medium, a shock wave is formed and the gas in the post-shock region is heated up to thermal Lorentz factors of $\gamma \sim \eta$, reconverting the kinetic energy of the shell into thermal energy of the particles. The thermal energy is radiated through synchrotron and inverse Compton processes at MeV to GeV energies. A non-uniform ambient medium can naturally lead to a multiply-peaked burst (e.g. Fenimore et al. 1996). Events of this class will have $\mathcal{A} < 0$, as in the case of trigger #2450, due to the effect of the prompt precursor. Hence, these $\mathcal{A} < 0$ events can be explained within the fireball model.

In other cases, the precursor can remain undetected but a multiply-peaked PAB can arise from internal shocks in bursts with several shells with different Lorentz factors (e.g. Kobayashi et al. 1997, Daigne & Mochkovitch 1998). In the simulations carried out by Kobayashi et al. (1997), bursts with negative skewness can be produced through multiple shell collisions (e.g. see Fig. 2f of their work).

Complex bursts, as the one shown in Fig. 1d, could be the result of instabilities on the expanding shell surface once it shocks the interstellar medium. Hydromagnetic instabilities in the contact discontinuity can lead to local variations in the fields and the flow's Lorentz factor, yielding very rapid changes in the time profiles (e.g. Daigne & Mochkovitch 1998). The resulting global morphology could resemble that seen in some bursts with negative skewness, such as #2240.

Single-peaked bursts with $\mathcal{A} < 0$, however, appear to be more difficult to explain with the fireball model. The main problem is that a single spike with slower rising than falling cannot be generated through dissipative shocks. In Fig. 4 we show BATSE trigger #444 (see also Table 3 and Fig. 1a). We have attempted to fit this event with the multiple shell model developed by Kobayashi et al. (1997). The γ-ray emission is produced when a shock results from the collision of two shells with different velocities. The randomized kinetic energy is then radiated through synchrotron and inverse Compton processes. Notice that the better the fit for the rising profile, the worse the model describes the fall. This is a straightforward consequence of the fact that cooling times are longer than particle acceleration times at the shock.

To better understand the meaning of the theoretical curves in Fig. 4 we recall the predicted luminosity in the case of a two shell interaction (Kobayashi et al. 1997),

$$\mathcal{L}(t) \propto \begin{cases} 1 - (1 + 2\gamma_m^2 ct/R)^{-2}, & 0 < t < \delta t_e / 2\gamma_m^2 \\ (1 + (2\gamma_m^2 t - \delta t_e)c/R)^{-2} - (1 + 2\gamma_m^2 ct/R)^{-2}, & t > \delta t_e/2\gamma_m^2 \end{cases} \quad (6)$$

where γ_m is the Lorentz factor of the merged shell (depending on the Lorentz factor and mass of each colliding shell), $\delta t_e/2\gamma_m^2$ is the time at which the burst reach its maximum, and R is the radius at which the collision takes place. Observational data of a given burst, its height and duration up to the maximum in the number of counts, allow a parameterization of $\mathcal{L}(t)$ with

$$B = \frac{2\gamma_m^2 c}{R}. \quad (7)$$

The shape of the pulse is asymmetric with a fast rise and a slower decline unlike a spike event with $\mathcal{A} < 0$. Attempts to fit such a burst using eq. (6) are shown in Fig. 4.

Spike-like bursts with $\mathcal{A} < 0$ are predicted, however, in some extrinsic models for GRBs. Torres et al. (1998a,b) have shown that microlensing effects produced upon the core of high redshifted AGNs by compact extragalactic objects which violate the weak energy condition at a macroscopic level would yield GRB-like lightcurves with spike-type profiles and negative skewness function. A similar burst with $\mathcal{A} > 0$ should be observed from several months up to a few years later in the same position of the sky, provided the lens has an absolute mass of the order of $1 M_\odot$. If this interpretation turns out to be correct, it could explain not just S-type PABs but also any apparent excess of positional coincidences among these bursts at a level compatible with current constraints on repetition over the whole sample. It would appear that the small group of spike bursts with negative skewness deserve further study.

6 CONCLUSIONS

GRBs exhibit a very rich variety of temporal profiles. Most of them have highly variable structure over timescales significantly shorter than the overall duration of the event. The study of burst morphology by Link and Epstein (1996) shows that a significant fraction of bursts ($\sim 1/3$) have time histories in which the flux rises more rapidly than it decays (PABs). Here we have argued that most PABs can be accommodated by fireball models. Isotropy and other average features, common to the bulk of observed bursts, are shared by PABs. But there is, however, a subclass of PABs, those which consist of a single, prominent peak with negative skewness, that appear to be inconsistent with the fireball mechanism. These events represent ~ 4 % of the total sample and certainly merit further research in order to clarify their nature.

ACKNOWLEDGMENTS

This research has made use of data obtained through the High Energy Astrophysics Science Archive Research Center, provided by the NASA/Goddard Space Flight Center and also of NASA/IPAC Extragalactic Database, which is operated by the Jet Propulsion Laboratory, California Institute of Technology, under contract with NASA. Our work has been supported by the Argentine agencies CONICET (D.F.T. and G.E.R - under grant PIP N^o 0430/98 -), ANPCT (G.E.R.), and FOMEC (L.A.A.). We acknowledge G. Bosch for his help in producing Fig. 2 and S. Grigera for an enlightening discussion on numerical issues.

REFERENCES

Balazs L. G., Mészáros A., Horvath I. 1998, A & A 339, 1
Briggs M. S. 1993, Ap. J. 407, 126
Briggs M. S. et al. 1996, Ap J 459, 40
Carter B. 1992, Ap J 391, L67
Cavallo G., Rees M. J. 1978, MNRAS 183, 359
Daigne F. and Mochkovitch 1998, MNRAS 296, 275
Djorgovski S. G. et al. 1997, Nature 387, 876
Fenimore F. E., Madras C. D., Nayakshin S. 1996, Ap J 473, 998
Fishman G. J., Meegan C. A. 1995, ARA & A 33, 415
Goodman J. 1986, Ap J 308, L47
Gorosabel J. et al. 1998, A & A 336, 57
Kobayashi S., Piran T., Sari R. 1997, Ap J 490, 92
Link B., Epstein R. I., Priedhorsky W. 1993, Ap J 408, L81
Link B., Epstein R. I. 1996, Ap J 466, 764
Meegan C. A., Fishman G. J., Wilson R. B. 1992, Nature 355, 143
Meegan C. A. et al. 1995, Ap J 446, L15
Melia F., Fatuzzo M. 1992, Ap J 398, L85
Mészáros P., Rees M. S. 1993, Ap J 405, 278
Mészáros P., Laguna P., Rees M. S. 1993, Ap. J. 415, 181
Mészáros P. 1997, Talk given at the 4th Hunstville Symposium on Gamma Ray Bursts, astro-ph 9711354.
Metzger M. R. et al. 1997, Nature 387, 878
Mitrofanov et al., (1994) in AIP Conf. Proc. 307, Gamma Ray Bursts, ed. G. J. Fishman , J. J. Brainerd & K. C. Hurley (New York: AIP), 187
Narayan R., Paczyński B., Piran T. 1992, Ap J 345, L83
Narayan R., Piran T. 1993, MNRAS 265, L65
Nemiroff R. J. et al. 1994, Ap J 423, 432
Paczyński B. 1986, Ap J 308, L43
Petrosian V, Efron B. 1995, Ap J 441, L37
Quashnock J. M., Lamb D. Q. 1993, MNRAS 265, L59
Tegmark M. et al. 1996, Ap J 466, 757
Torres D. F., Romero G. E. and Anchordoqui L. A. 1998a, Mod. Phys. Lett. A13, 1575
Torres D. F., Romero G. E. and Anchordoqui L. A. 1998b, Phys. Rev. D58, 123001
Usov V. 1992, Nature 357, 472
van Paradjis J. et al. 1997, Nature 386, 686
Wang V. C., Lingenfelter R. E. 1995, Ap J 441, 747
Woosley S. 1993, Ap J 405, 273

Table 1. GRBs with negative skewness function for all four cut-off parameters. Type 1 indicates bursts whose errors in $\mathcal{A}$ are less than the modulus of $\mathcal{A}$ itself and type 2 indicates cases in which at least one of the computed errors in $\mathcal{A}$ exceeds the modulus of $\mathcal{A}$. S, M, and C stand for single, multiply-peaked and complex temporal profiles.

Peak flux	#	Type	$\mathcal{A}_{f_1}$	$\mathcal{A}_{f_2}$	$\mathcal{A}_{f_3}$	$\mathcal{A}_{f_4}$	Profile
20.23800	1663	1	-9.55E-02 ± 1.92E-03	-0.14 ± 2.56E-03	-0.17 ± 1.13E-02	-0.15 ± 5.21E-02	M
20.13300	219	1	-0.20 ± 9.21E-03	-0.20 ± 8.48E-03	-1.1 ± 4.06E-02	-0.15 ± 6.84E-02	M
13.78700	1122	1	-0.30 ± 7.69E-02	-0.72 ± 0.10	-0.21 ± 5.82E-02	-0.72 ± 0.15	M
8.79800	2834	1	-4.42E-02 ± 2.86E-02	-6.20E-02 ± 4.02E-02	-8.69E-02 ± 5.62E-02	-0.13 ± 8.24E-02	M
8.27700	2450	1	-0.42 ± 9.27E-03	-7.51E-02 ± 3.24E-03	-0.25 ± 6.46E-03	-0.65 ± 9.21E-02	M
7.13100	2852	2	-0.15 ± 8.97E-03	-1.17E-02 ± 4.13E-02	-5.91E-02 ± 5.27E-02	-0.16 ± 0.46	M
6.71400	2436	1	-0.71 ± 8.86E-02	-2.87E-02 ± 5.27E-03	-0.27 ± 7.69E-02	-0.48 ± 1.95E-02	M
5.69900	1974	1	-9.82E-02 ± 8.65E-03	-0.15 ± 8.49E-03	-0.36 ± 0.16	-4.31E-02 ± 3.76E-02	M
5.24900	179	1	-0.62 ± 9.11E-02	-0.73 ± 0.24	-0.18 ± 5.49E-02	-0.27 ± 0.12	S
4.53800	222	2	-0.82 ± 0.22	-0.18 ± 3.41E-02	-0.23 ± 7.24E-02	-0.11 ± 0.15	M
3.02000	2922	2	-0.35 ± 1.80E-02	-0.53 ± 0.14	-0.13 ± 0.11	-0.32 ± 0.43	C
2.79600	906	2	-9.97E-02 ± 6.91E-02	-0.11 ± 5.89E-02	-0.22 ± 0.16	-0.18 ± 0.19	S
2.34200	2428	2	-0.14 ± 7.57E-03	-8.68E-02 ± 8.95E-02	-0.13 ± 2.24E-02	-0.52 ± 4.63E-02	M
2.06600	2476	1	-2.28E-02 ± 2.35E-03	-5.84E-03 ± 4.12E-03	-0.11 ± 3.35E-02	-0.20 ± 3.06E-02	M
1.71900	353	2	-0.23 ± 2.14E-02	-0.13 ± 3.25E-02	-9.92E-02 ± 1.86E-02	-0.12 ± 0.28	S
1.64800	2074	1	-9.33E-02 ± 4.34E-02	-0.19 ± 9.48E-02	-0.31 ± 0.11	-0.25 ± 0.20	M
1.54500	254	2	-3.68E-02 ± 7.61E-02	-6.36E-02 ± 8.59E-02	-0.15 ± 0.19	-0.19 ± 0.36	S
1.44900	1197	2	-0.27 ± 4.82E-02	-0.29 ± 0.14	-0.17 ± 17	-0.25 ± 0.27	C
1.37400	1413	2	-0.18 ± 0.20	-0.29 ± 0.24	-2.68E-02 ± 0.30	-0.14 ± 0.27	M
1.35300	2610	1	-0.31 ± 3.31E-02	-0.19 ± 3.28E-02	-0.87 ± 6.81E-02	-0.39 ± 0.21	C
1.11400	752	2	-0.19 ± 0.14	-0.24 ± 0.13	-0.61 ± 0.29	-0.32 ± 0.34	S
1.11000	2828	2	-7.11E-02 ± 0.29	-9.19E-02 ± 9.92E-02	-0.14 ± 0.16	-0.15 ± 0.27	C
0.84500	2448	2	-9.77E-02 ± 1.87E-02	-0.11 ± 2.28E-02	-7.29E-03 ± 7.45E-02	-0.11 ± 8.27E-02	C
0.77600	2495	1	-2.43E-02 ± 1.23E-02	-4.93E-02 ± 1.22E-02	-0.15 ± 0.14	-1.20 ± 0.68	C
0.66100	690	2	-0.63 ± 0.21	-0.35 ± 0..32	-0.19 ± 0.37	-0.30 ± 0.46	C
0.59400	2442	2	-2.36E-02 ± 3.01E-02	-1.03E-02 ± 0.11	-0.13 ± 0.17	-0.22 ± 0.14	C

Table 2. GRBs with negative skewness for three thresholds f. For f_4, these bursts did not fulfill the criteria for the assignment of an $\mathcal{A}$ value. Burst type and capital letters have the same meaning as in Table 1.

Peak flux	#	Type	$\mathcal{A}_{f_1}$	$\mathcal{A}_{f_2}$	$\mathcal{A}_{f_3}$	Profile
12.45800	1440	1	-7.47E-02 ± 8.56E-03	-0.15 ± 8.27E-03	-0.35 ± 0.17	M
8.73700	2799	1	-0.78 ± 6.23E-03	-1.1 ± 0.23	-0.29 ± 8.58E-02	M
2.37600	2861	2	-2.27E-02 ± 7.87E-02	-0.12 ± 0.12	-7.99E-02 ± 0.27	M
2.35100	2795	1	-0.13 ± 1.62E-02	-0.14 ± 1.92E-02	-0.14 ± 5.31E-02	S
2.00500	1359	2	-0.11 ± 0.14	-0.14 ± 8.14E-02	-0.76 ± 0.27	S
1.93900	1154	2	-6.24E-02 ± 6.27E-02	-8.17E-02 ± 6.22E-02	-0.44 ± 0.24	S
1.23000	1924	1	-0.22 ± 0.12	-0.16 ± 0.11	-0.17 ± 0.13	S
1.22600	1611	2	-0.73 ± 0.34	-0.20 ± 0.29	-0.56 ± 0.26	C
1.20400	3012	2	-2.87E-02 ± 0.12	-0.15 ± 0.16	-9.32E-02 ± 0.22	M
1.20200	3080	2	-0.90 ± 0.36	-0.17 ± 0.20	-0.57 ± 0.25	C
1.19100	2040	2	-4.77E-02 ± 0.16	-5.50E-02 ± 0.18	-8.62E-02 ± 0.25	C
1.05000	3017	2	-6.30E-02 ± 0.10	-0.17 ± 0.17	-0.10 ± 0.19	C
0.88000	2204	2	-9.25E-02 ± 0.28	-0.41 ± 0.31	-0.29 ± 0.22	C
0.81300	2240	2	-0.18 ± 3.84E-02	-0.20 ± 5.62E-02	-0.10 ± 0.12	C
0.74000	114	2	-0.13 ± 0.12	-0.11 ± 0.28	-0.38 ± 0.45	C
0.67800	2434	1	-0.31 ± 2.74E-02	-0.37 ± 3.15E-02	-1.0 ± 0.24	S
0.54600	2727	2	-7.14E-03 ± 0.11	-1.43E-02 ± 8.57E-02	-0.33 ± 0.50	C
0.34200	1435	2	-0.15 ± 0.25	-0.48 ± 0.23	-0.65 ± 0.26	C

Table 3. GRBs with $\mathcal{A} < 0$ for two thresholds.

Peak flux	#	Type	$\mathcal{A}_{f_1}$	$\mathcal{A}_{f_2}$	Profile
28.55900	444	1	-0.23 ± 1.66E-02	-0.45 ± 3.51E-02	S
4.25500	2993	2	-0.53 ± 0.58	-9.09E-02 ± 5.33E-02	M
3.26900	2041	1	-0.61 ± 8.86E-02	-1.1 ± 0.36	M
2.22800	2220	2	-0.44 ± 0.46	-1.66E-02 ± 0.15	S
1.89300	2201	1	-0.26 ± 0.15	-0.32 ± 7.65E-02	S
1.85500	2788	2	-4.68E-02 ± 0.10	-5.79E-02 ± 1.80E-02	S
1.22900	1142	1	-0.83 ± 0.39	-1.1 ± 0.42	S
1.20400	1968	1	-0.26 ± 0.19	-0.29 ± 0.14	S
1.07700	171	2	-7.18E-02 ± 0.26	-9.49E-02 ± 0.27	C
1.06800	2529	1	-0.40 ± 5.15E-02	-0.35 ± 0.11	M
1.06000	2853	2	-3.79E-02 ± 9.67E-02	-8.85E-02 ± 0.14	C
0.96700	237	2	-0.11 ± 0.57	-0.38 ± 0.46	C
0.97900	2800	1	-0.21 ± 0.12	-0.27 ± 0.17	C
0.82500	2290	1	-0.47 ± 4.08E-02	-0.52 ± 4.27E-02	C
0.80800	2129	2	-2.30E-02 ± 0.20	-0.16 ± 0.23	C
0.78200	1192	2	-2.31E-02 ± 0.13	-3.93E-02 ± 0.20	C
0.78800	2857	1	-0.25 ± 0.16	-0.32 ± 0.18	C
0.76600	1430	2	-8.19E-02 ± 0.26	-0.10 ± 0.24	C
0.71600	1404	2	-1.62E-02 ± 0.17	-1.85E-02 ± 0.22	C
0.71300	1110	2	-0.11 ± 0.14	-1.73E-02 ± 0.14	C
0.70800	204	2	-0.25 ± 0.10	-0.11 ± 0.14	M
0.70400	2776	1	-0.23 ± 8.03E-02	-0.22 ± 0.10	C
0..65400	2996	2	-0.17 ± 0.23	-4.76E-02 ± 0.48	C
0.65100	2725	1	-0.25 ± 8.81-02	-0.40 ± 0.19	C
0.61800	1655	2	-7.66E-02 ± 0.31	-0.37 ± 0.28	C
0.57600	2750	2	-4.14E-02 ± 0.13	-0.11 ± 5.83E-02	C
0.56300	2230	2	-0.10 ± 0.20	-0.14 ± 0.18	C
0.56100	2069	2	-9.99E-02 ± 0.15	-0.37 ± 0.20	C
0.55200	1382	2	-0.14 ± 0.18	-0.28 ± 0.16	C
0.54500	2900	2	-0.33 ± 0.24	-0.12 ± 0.30	C
0.53400	1465	2	-8.62E-02 ± 0.23	-2 ± 0.34	C
0.49800	2233	1	-0.48 ± 0.38	-0.51 ± 0.13	C
0.47500	559	1	-0.49 ± 0.31	-0.31 ± 0.24	C
0.44000	1120	2	-1.27E-02 ± 0.19	-7.57E-03 ± 0.22	C

Table 4. GRBs with $\mathcal{A} < 0$ for one threshold.

Peak flux	#	Type	$\mathcal{A}_{f_1}$	Profile
8.76100	2978	1	-1.60 ± 0.95	S
5.57300	551	1	-9.78E-02 ± 5.33E-02	S
4.68100	1851	1	-1.1 ± 0.44	S
4.08600	2995	1	-0.83 ± 0.25	S
3.43700	2918	1	-0.24 ± 0.20	S
2.97900	297	1	-0.11 ± 3.65E-02	M
1.92600	2161	1	-1.0 ± 0.63	S
1.79100	2846	1	-0.36 ± 0.18	S
1.67000	1461	1	-0.95 ± 0.41	S
1.13300	2163	2	-0.13 ± 0.13	S
1.03200	2823	2	-0.32 ± 0.34	S
0.69500	2508	1	-1.6 ± 0.74	C
0.64800	2437	1	-0.17 ± 4.50E-02	C

Table 5. Mean values of hardness ratio and temporal durations for type 1 PABs compared with usual $\mathcal{A} > 0$ bursts. All bursts have $\mathcal{A}_{f_i}$ computed for all four f_i analysed. The PAB group has ∼26 bursts, whereas the $\mathcal{A} > 0$ set comprises ∼100 of the total sample.

	<Hard. Ratio>	σ	$< T_{90} >$	σ
type 1= PABs	3.6	2.3	35	42
type 1= GRBs	3.2	1.5	49	50

Table 6. Isotropy characteristics. The expected values of the statistics (corrected for BATSE exposure) are -0.013 for $< \cos\theta >$ and -0.005 for $< \sin^2 b - 1/3 >$.

Sample	$< \cos\theta >$	$\sigma = 0.99\sqrt{1/3N_B}$	$< \sin^2 b - 1/3 >$	$\sigma = 0.99\sqrt{4/45N_B}$
1+2-types=91 GRBs	-0.034	0.059	-0.023	0.030
1-type=41 GRBs	0.003	0.089	-0.045	0.046
2-type=49 GRBs	-0.065	0.082	-0.005	0.042
1-type Table 1=12 GRBs	-0.120	0.165	-0.052	0.085
1-type Table 3=13 GRBs	0.072	0.158	-0.092	0.081
1-type Table 1+ 2=17 GRBs	0.030	0.138	-0.104	0.071
1-type Table 1 + 2 + 3=30 GRBs	-0.014	0.104	-0.098	0.053
single-peaked =26 GRBs	0.015	0.110	0.015	0.057
Multiply-peaked and complex =65 GRBs	-0.045	0.071	-0.044	0.036

Figure 1. Examples of bursts with negative skewness. From top to bottom and left to right, Fig. 1a and 1b are single-peaked bursts. Fig. 1c is an example of a multiply-peaked burst with $\mathcal{A} < 0$ and Fig. 1d is a complex peculiar asymmetric burst. For details on the particular $\mathcal{A}$-values see Tables 1 - 4.

Figure 2. Spatial position (Galactic coordinates, Aitoff projection) of the PABs presented in Tables 1 - 4. The sky distribution is consistent with perfect isotropy.

Figure 3. An example of a burst with negative overall skewness, but positive skewness for the subpeaks. A burst of this type could be made up of a precursor associated with baryonic pollution, followed by a series of peaks generated in the collision of a relativistic shell with the interstellar medium.

Figure 4. An illustration of the inconsistency between the fireball model and spike bursts with negative skewness. Shown is the spike burst of Fig. 1a (see also Table 3). The bar plot stands for the observed number of counts. We also show several profiles of the light curves predicted by the multiple shell model of Kobayashi et al. (1997) corresponding to $B = 0.1, 5$ and 15 (see text). In general, the better the theoretical curves fit the rising curve, the worse they fit the falling portion.

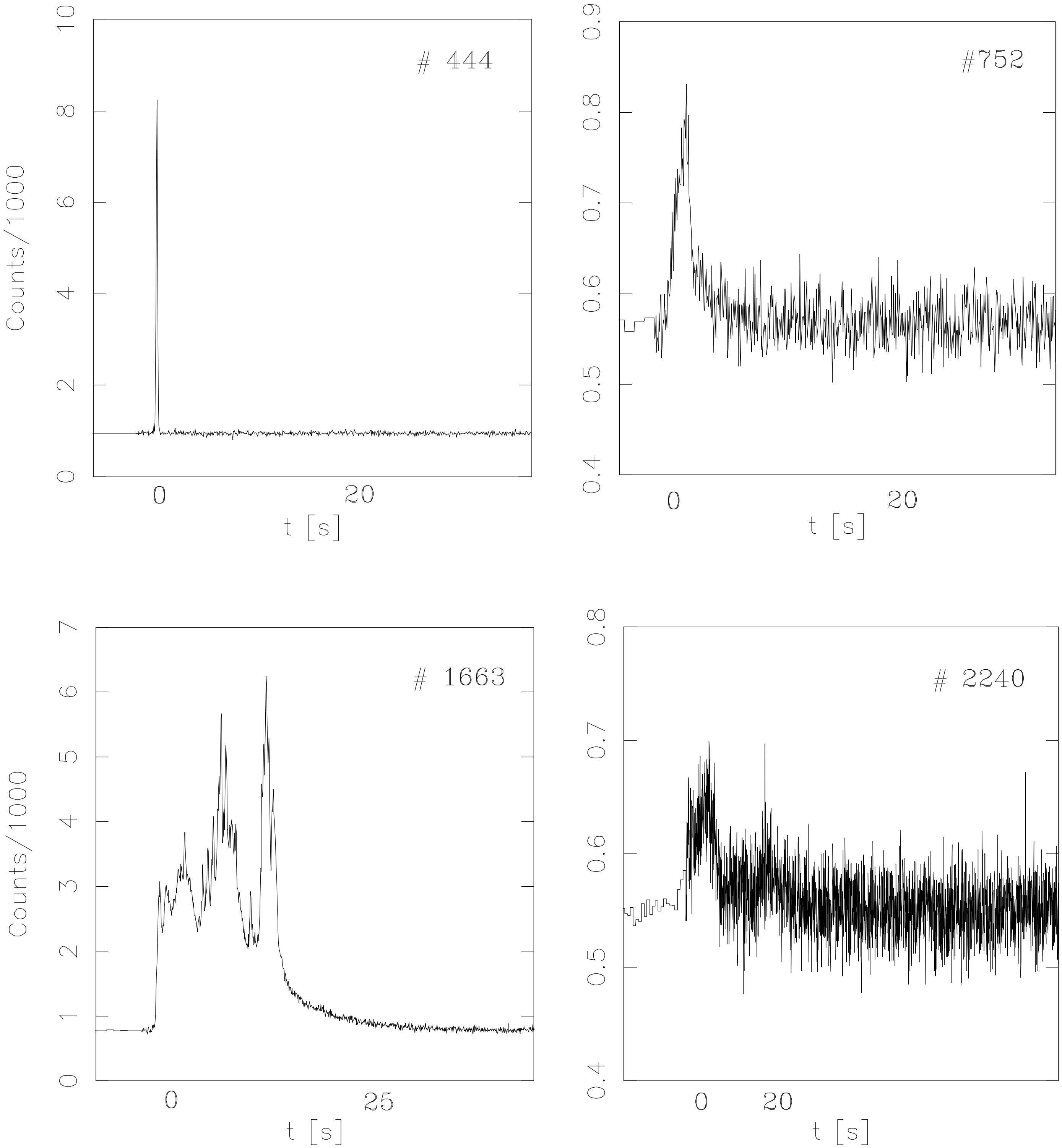

444
Counts/1000
t [s]
#752
t [s]
1663
Counts/1000
t [s]
2240
t [s]

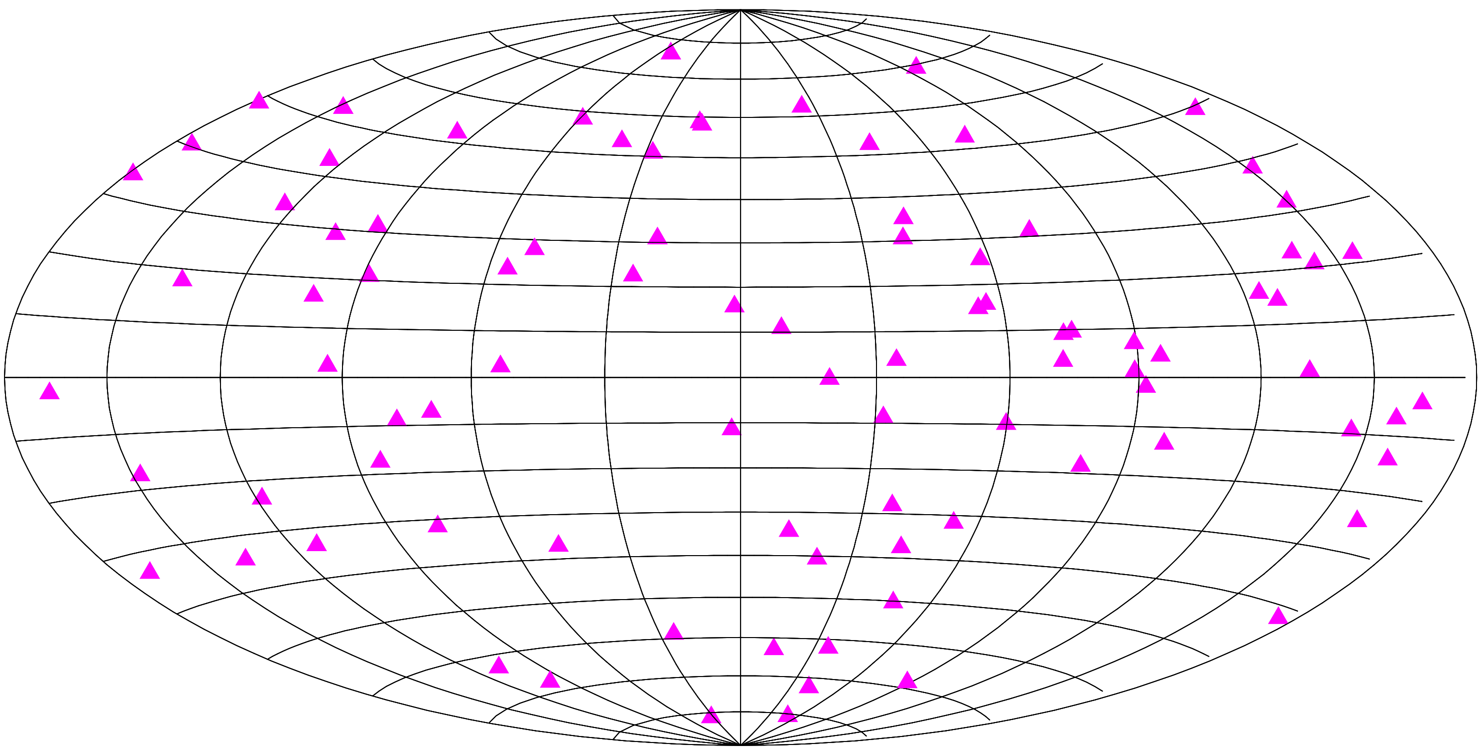

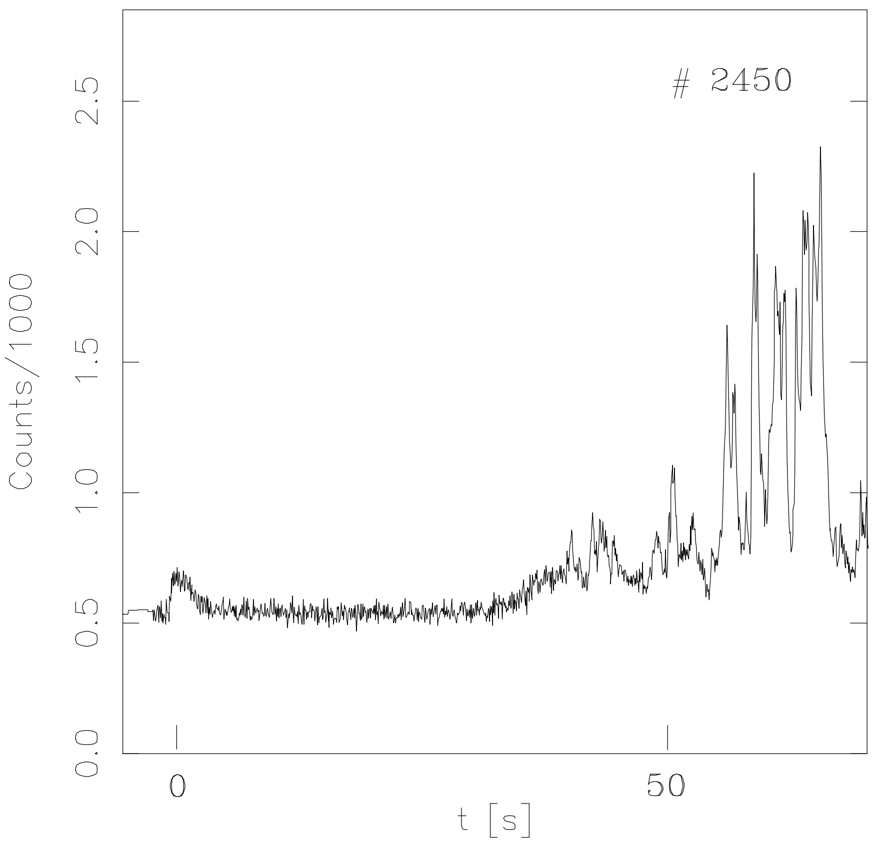

2450
Counts/1000
0.0
0.5
1.0
1.5
2.0
2.5
0
50
t [s]

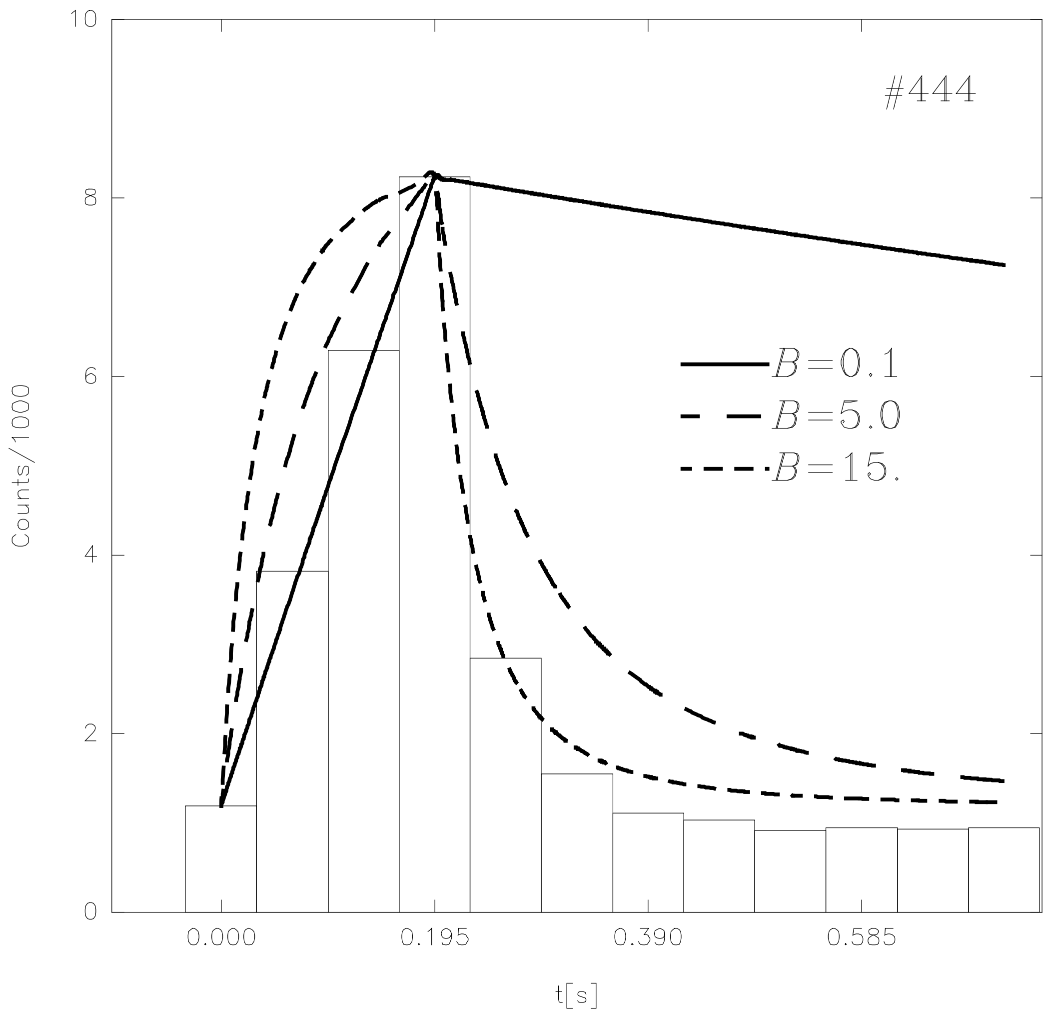
#444
B=0.1
B=5.0
B=15.
Counts/1000
t[s]
0.000
0.195
0.390
0.585
0
2
4
6
8
10